



RESEARCH ARTICLE

A GHz chirped amplitude-modulated laser for high-contrast plasma gratings

Michael Valdman¹, Amir Hen, and Gilad Marcus¹

Applied Physics Institute, Hebrew University of Jerusalem, Jerusalem, Israel

(Received 1 September 2023; revised 21 October 2023; accepted 9 November 2023)

Abstract

The generation and control of large amplitude plasma gratings and other plasma structures is of paramount importance for the realization of plasma photonics. Autoresonant excitation of such structures by means of chirped amplitude-modulated lasers has been recently discussed and analyzed theoretically. Here we discuss the parameter space for the realization of such a scheme and describe the laser system that was built towards this goal. We also expand our earlier theoretical study to account for the more realistic case of a moderately focused laser beam, instead of the simplified plane wave approximation.

Keywords: amplitude modulation; high-frequency modulation; autoresonance; ion acoustic wave

1. Introduction

In recent years, there has been an increased interest in the interaction of light with structured plasma. For example, plasma gratings may be used for short pulse amplification and the compression of high-power chirped pulses^[1,2], transient plasma photonic crystals used as a high reflector^[3], plasma-based optical components such as lenses, diffractive and holographic lenses^[4–6], polarization optics^[7–9], crossed-beam energy re-distribution for symmetry control in inertial confinement fusion (ICF)^[10] and crossed-beam depolarization for mitigating parametric instabilities in ICF^[11]. Currently, the efficiency of the above-mentioned applications is poor. One of the main reasons for the low efficiency of these schemes is the difficulty of controlling these plasma structures as they are driven into the nonlinear regime. To overcome this limitation, we proposed to drive a high-amplitude, standing ion acoustic wave (SIAW) by the interaction of a plasma medium with two counter-propagating laser beams that are amplitude modulated with a slowly varying frequency^[12]. The beating frequency of the chirped two counter-propagating beams starts slightly off the linear resonance of an ion acoustic wave, and then slowly sweeps through it. If the chirp rate is slow enough, the plasma oscillations are automatically phase-locked to the beating frequency and stay in resonance. This process is known as

autoresonance (AR). AR is a proven and general technique of exciting an oscillatory nonlinear system into high energies by a weak chirped driving oscillation^[13–15]. This method is general and has been applied in many fields of physics, such as particle accelerators, coherent control of molecular vibration states^[14–17], fluid dynamics^[18], plasmas^[19], nonlinear waves^[20] and planetary dynamics^[21].

In this paper, we follow our previous theoretical proposal^[12] and report on the development of a laser system to drive the SIAW and push it into the nonlinear regime where the amplitude of the acoustic wave could reach a significant fraction of the unperturbed plasma density. This laser is designed with the ability to arbitrarily modulate its amplitude with a modulation frequency of up to a few GHz. For the purpose of driving the SIAW into high energies, we chirped the amplitude modulation from about 500 MHz to more than 3.5 GHz. It is worth mentioning here that such a laser may be useful for other applications, such as the chirped amplitude modulation laser radar (LADAR) for range and Doppler measurements and for 3D imaging^[22].

The paper is organized as follows. In **Section 2**, we analyze the parameter space for generating the SIAW and the required laser parameters. In **Section 3**, we describe our laser system. Next, with the analysis of **Section 2** and the available laser parameters (**Figure 1**), we show that a moderate focusing of the laser is needed for attaining the AR threshold intensity, and our plane wave approximation in Ref. [12] might not be valid. In the Appendix, we take our previous plane wave approximation and extend it to the more realistic case of focused laser beams with a finite waist.

Correspondence to: Gilad Marcus, Applied Physics Institute, Hebrew University of Jerusalem, 91904 Jerusalem, Israel. Email: gilad.marcus@mail.huji.ac.il

© The Author(s), 2023. Published by Cambridge University Press in association with Chinese Laser Press. This is an Open Access article, distributed under the terms of the Creative Commons Attribution licence (<https://creativecommons.org/licenses/by/4.0/>), which permits unrestricted re-use, distribution and reproduction, provided the original article is properly cited.

2. Parameter space of the experiment

In all autoresonant driving schemes, the driver frequency is slowly varying, passing through the zero-amplitude natural frequency of the system, and if the driving force exceeds a certain threshold, the nonlinear system is automatically phased-locked with the driver frequency. In that case, the resonance condition $\omega_d(t) - \Omega(A) = 0$ is kept during the whole excitation process, where $\omega_d(t) = \Omega_0 - \alpha t$ is the time-dependent driving frequency, Ω_0 is the zero-amplitude natural frequency of the system and $\Omega(A) = \Omega_0 - \beta A^2$ is the amplitude-dependent natural frequency of the nonlinear system. Thus, the amplitude A grows in time according to $A(t) = \sqrt{\frac{\omega_d(t) - \Omega_0}{\beta}} = \sqrt{\frac{\alpha t}{\beta}}$. The threshold of the AR obeys a general power law that applies to all AR cases:

$$\varepsilon_{\text{th}} = \eta \frac{\alpha^{3/4}}{\sqrt{\beta}}, \quad (1)$$

where η is a constant of the order of 0.5 and α and β are the chirp rate and the nonlinear coefficient of the amplitude-dependent resonance (often given as dimensionless parameters), respectively. In our theoretical paper on AR excitation of SIAWs^[12] we used dimensionless variables and parameters, such that the time, the position and the velocity are normalized with respect to the inverse ion plasma frequency $\omega_{\text{pi}}^{-1} = \sqrt{\varepsilon_0 m_i / n_e e^2}$, the Debye length $\lambda_D = \sqrt{\varepsilon_0 T_e / n_e e^2}$ and the modified electron thermal velocity $\left(\frac{m_e}{m_i}\right)^{1/2} u_e$. The plasma density and the electric potential are normalized with respect to the unperturbed plasma density and $k_B T_e / e$.

To realize AR-driven SIAWs in the laboratory, we have to choose the right conditions, such as the plasma density, electron temperature, ion mass and driving frequency chirp rate, to fit within the experimental limitations. A prerequisite for the success of the experiment is a laser driver with intensity above the AR threshold. One way to keep this AR threshold low is to reduce the chirp rate, α (see Equation (1)). However, the wave amplitude is growing in time according to $A(t) = \sqrt{\alpha t / \beta}$; thus, to attain the same amplitude with a lower chirp rate, we need a longer pulse duration. These limitations combine with other technical limitations to form a parameter space from which we have to pick the optimal conditions for SIAW AR excitation. Our laser system (see the next section) consists of a seeding laser that is amplitude modulated by an electro-optic Mach–Zehnder interferometer (iXblue), driven by an arbitrary waveform generator (AWG) and amplified in a regenerative amplifier^[23].

We choose to set our laser wavelength at 1064 nm since both seeding lasers are abundant, fast electro-optical modulators are available and there are efficient neodymium-doped yttrium aluminum garnet (Nd:YAG) amplifiers. This wavelength choice imposes the wavelength of the ion acoustic

wave to be half of the laser wavelength ($\lambda_{\text{IAW}} = 532$ nm). The laser cavity length imposes an upper-bound limitation on the pulse duration. In our case, the cavity allowed for a pulse duration of approximately 35 ns (a schematic of our zig-zag folded 5.1 m long cavity is given in Figure 2). Due to space limitations on the optical table, a substantial longer cavity will require our cavity to be folded many times. This in turn will increase optical losses, reduce cavity stability and complicate cavity alignment, which is already a problem with such a long cavity. The AWG puts an upper-bound limitation of approximately 4.5–5 GHz on the modulation frequency. Such a modulation will broaden the laser spectrum by not more than 0.02 nm, well within the Nd:YAG gain bandwidth. Therefore, no effect on the laser efficiency is expected, nor is observed. Figure 1 shows a selection chart that can help us identify the optimal experimental conditions. Figures 1(a) and 1(b) show that the energy threshold and the time window are equal to $10/\sqrt{\alpha}$, both of which are needed for efficient AR excitation^[13]. It also shows the swept bandwidth within a time window of 35 ns, which puts an upper bound on the SIAW amplitude (Figure 1(c)) and the linear ion acoustic wave frequency (Figure 1(d)). The gray areas indicate the working area imposed by the above-mentioned limitations. From Figure 1 we first realize that the linear SIAW frequency for the case of helium ions is too high for our current AWG; therefore, we aim at working with neon ions at densities of around $10 \times 10^{17} \text{ cm}^{-3}$ and dimensionless chirp rates in the range of $1 \times 10^{-6} - 3 \times 10^{-6}$ (which should be multiplied by ω_{pi}^2 to translate into the dimensional chirp rate).

3. Laser system

According to our analysis in Section 2, our laser should have the following parameters: central wavelength $\lambda_c = 1064$ nm, pulse duration $\tau_p \cong 35$ ns, amplitude modulation with chirped frequency spanning from 3 to 1.2 GHz within the pulse duration, that is, a chirp rate of approximately equal to 0.0514 ns^{-2} , and an energy/pulse of approximately equal to 2.5–3 mJ, provided that we focus the beam to a spot waist of 30–35 μm . Because of the high modulation frequency and the demand for sweeping a large bandwidth within the pulse duration, we choose to shape our pulse by using a high-frequency LiNbO₃ waveguide Mach–Zehnder modulator (iXblue). The laser system starts from a fiber-coupled narrow bandwidth distributed feedback (DFB) laser diode, having a central wavelength of 1064.5 nm and an average power of 150 mW. This seed is sliced into a square pulse of about 20–35 ns and amplitude modulated with a chirped quasi-sinusoidal shape at frequencies ranging from approximately 4 GHz to a few hundred MHz. The exact pulse-shape is imposed by an arbitrary wave generator that feeds the Mach–Zehnder modulator.

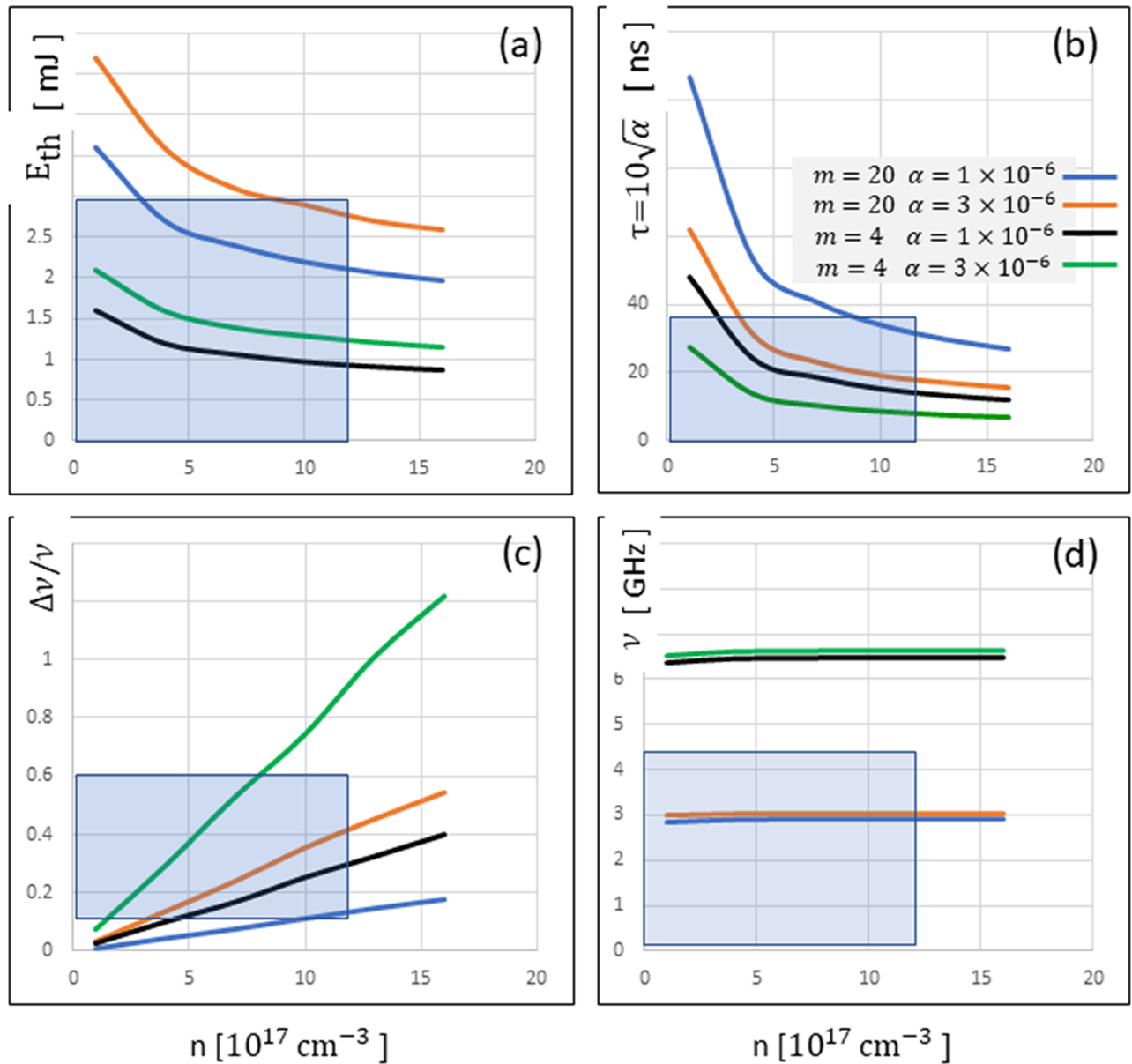


Figure 1. A selection chart for the best experimental conditions. (a) The pulse energy threshold (in mJ) as a function of the plasma density (in units of 10^{17} cm^{-3}), assuming a beam waist of $35 \mu\text{m}$. (b) The time window $10/\sqrt{\alpha}$ (in ns) as a function of the plasma density. (c) The swept bandwidth within the time window of 35 ns. (d) The linear ion acoustic wave frequency (GHz). The laser wavelength is chosen to be $\lambda_L = 1064 \text{ nm}$ and the electron temperature is 0.5 eV. Orange and blue lines represent the ion mass of 20 a.u. (neon) and the dimensionless chirp rate of 1×10^{-6} or 3×10^{-6} , respectively. Green and black lines represent the ion mass of 4 a.u. (helium) and the dimensionless chirp rate of 1×10^{-6} or 3×10^{-6} , respectively.

To reach the AR threshold, we have to amplify the shaped 3 nJ seed by about six orders of magnitude. A regenerative amplifier^[23] could fill this energy gap while supporting a good beam profile. Nevertheless, the need for high pulse energy/high laser power and maintaining the required time structure of the pulse imposes some challenges. The first challenge is to inject the seed pulse into the regenerative amplifier, lock it inside the cavity and amplify it while preserving its shape and avoiding clipping it. In a common regenerative design^[23] (see Figure 2(a)), the seed is reflected from a polarizer into the cavity, passing through a quarter

waveplate (QWP) and a passive Pockels cell, reflected from the first end mirror of the cavity (M1) towards the second end mirror (M4). While going towards the second end mirror, it goes again through the passive Pockels cell and the QWP. Once the tail of the pulse passes the second time through the Pockels cell, it is possible to switch on the Pockels cell and lock the pulse inside the cavity, but care should be taken not to clip at this time the head of the pulse. Since our pulse duration is designed to be in the region of 35 ns, the distance from the Pockels cell to the second end mirror and back to the Pockels cell should be around 11 m. Such a long

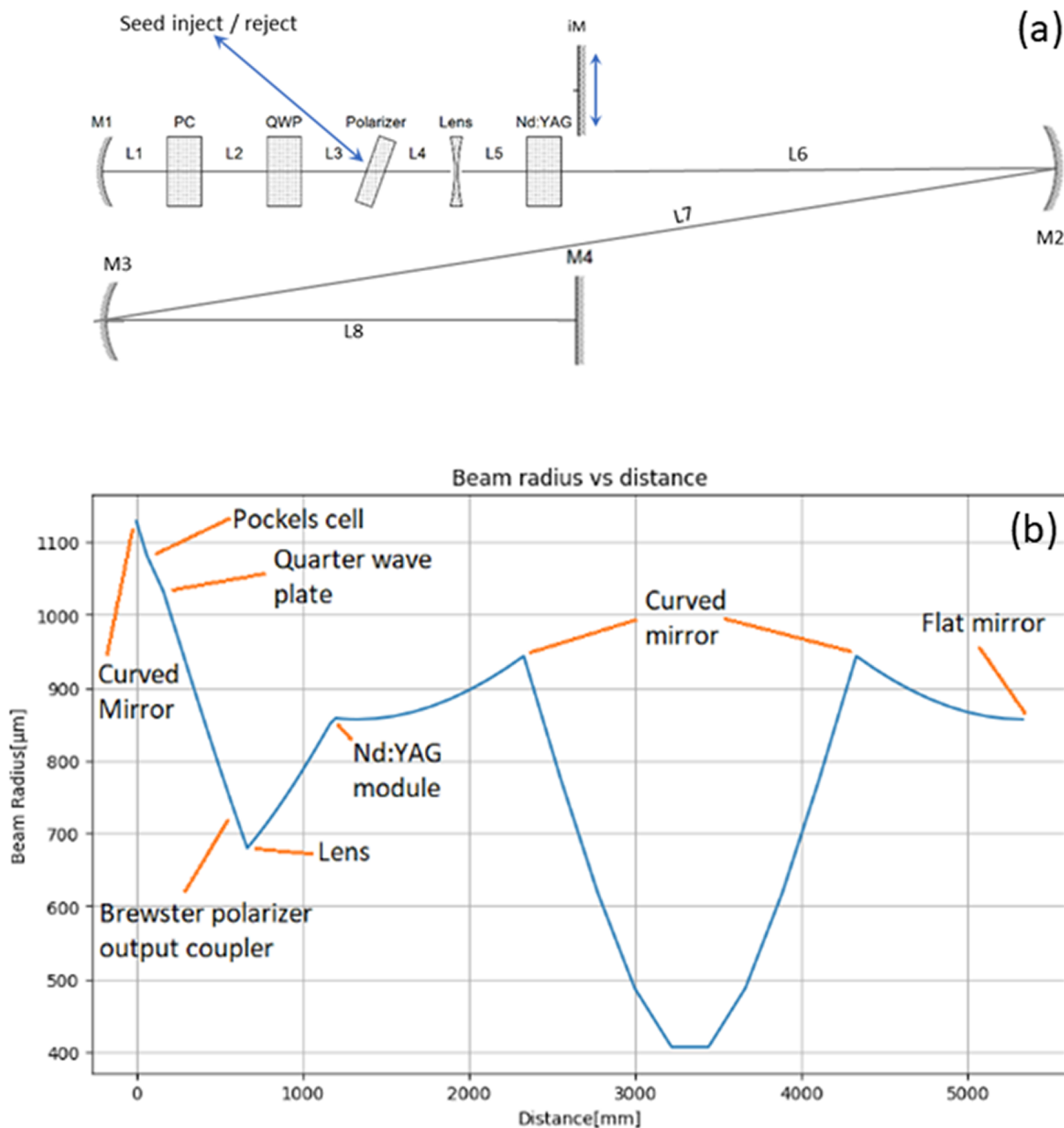


Figure 2. (a) Schematic of cavity design. M1, spherical front end-mirror with radius of 3 m; L1, 63 mm; PC, Pockels cell; L2, 60 mm; QWP, quarter waveplate; L3, 340 mm; L4, 10 mm; lens, focal length -750 mm; L5, 500 mm; Nd:YAG, gain medium; iM, removable flat mirror used as the back end-mirror of the short cavity; L6, 1.1 m; M2 and M3, spherical mirrors with radius of 2 m; L7, 2 m; L8, 1 m; M4, flat mirror used as the end-mirror of the long cavity. (b) Caustic of the beam inside the cavity obtained from simulations with ReZonator 2^[24].

cavity poses difficulties in aligning it and keeping it stable. To extract high power out of it is even more challenging because of the thermal lensing effect. Figure 2(a) shows a schematic of our regenerative cavity. Our guidelines in the design of the cavity were as follows: (i) make it long enough to accommodate the approximately 35 ns pulse without clipping it; (ii) position the Pockels cell where the beam waist is large enough to avoid damages to the Pockels cell; (iii) position the gain medium (Northrop Grumman, diode-pumped, Nd:YAG rod, 2 mm diameter and length of 63 mm)

where the beam waist is filling the entire Nd:YAG rod cross-section in order to extract as much energy as possible; (iv) the cavity should be stable for a large range of thermal lensing (see Figure 3); (v) there should be easy alignment of the cavity.

We used ReZonator 2^[24] to analyze the caustic of the beam inside the cavity (Figure 2(b)) and the cavity stability as a function of the gain medium thermal lensing (Figure 3). To calculate the stability of the cavity with respect to the thermal lensing, we modeled the thermal lensing effect by

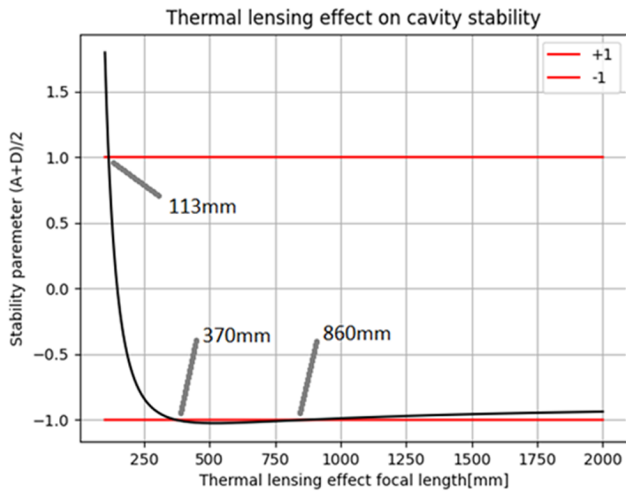


Figure 3. The cavity stability parameter as a function of the effective thermal lensing (black). The red lines indicate the limits of stability.

virtually placing a lens inside the Nd:YAG rod with the focal length as a variable parameter and calculated the stability parameter $(A + D) / 2$ as a function of the focal length, where A and D are the diagonal elements of the $ABCD$ ray transfer matrix for a complete roundtrip inside the cavity (see Figure 3). According to this calculation, our cavity is stable within the range of thermal lensing $f = \infty \rightarrow f = 860$ mm. For stronger thermal lensing, there is a range between 860 and 370 mm in which the cavity loses its stability, and in

between 370 and 113 mm it is stable again. We aim to work at conditions of moderate thermal lensing; therefore, with a stable range spanning from $f = \infty$ to $f = 860$ mm.

The cavity length as given in Figure 2 is 5.3 m. To align such a long cavity and find the optimal cavity arrangement is not easy. To overcome this problem, we used a modular approach. We first built a short cavity by inserting a flat-end mirror right after the gain medium (see the iM mirror in Figure 2(a)) and optimized the approximately 1 m long cavity. Once this cavity is perfected, we put an iris around the leaked beam from the flat-end mirror and imaged it with a 4f, 4-m long telescope on another flat mirror. With this flat mirror we retroreflect the beam back through the iris, then remove the iM mirror and form the 5.3 m long cavity.

Figures 4–6 show the chirped modulated signal from the AWG, along with the output from the regenerative amplifier. Comparing the AWG signal to the amplified optical pulse, we can see a slight square wave distortion of the envelope in which the tail of the pulse experiences a lower gain than the head of the pulse.

This distortion could be compensated by shaping the pulse with the AWG, but it is not really important for the purpose of AR excitation since the AR threshold is mainly important at the beginning of the pulse. Besides this distortion, we see that the amplitude modulated high frequencies and the chirp rate are well preserved during the six-order of magnitude amplification. The average output power is about 1 W at the optimal repetition rate of 400 Hz, that is, about 2.5 mJ/pulse.

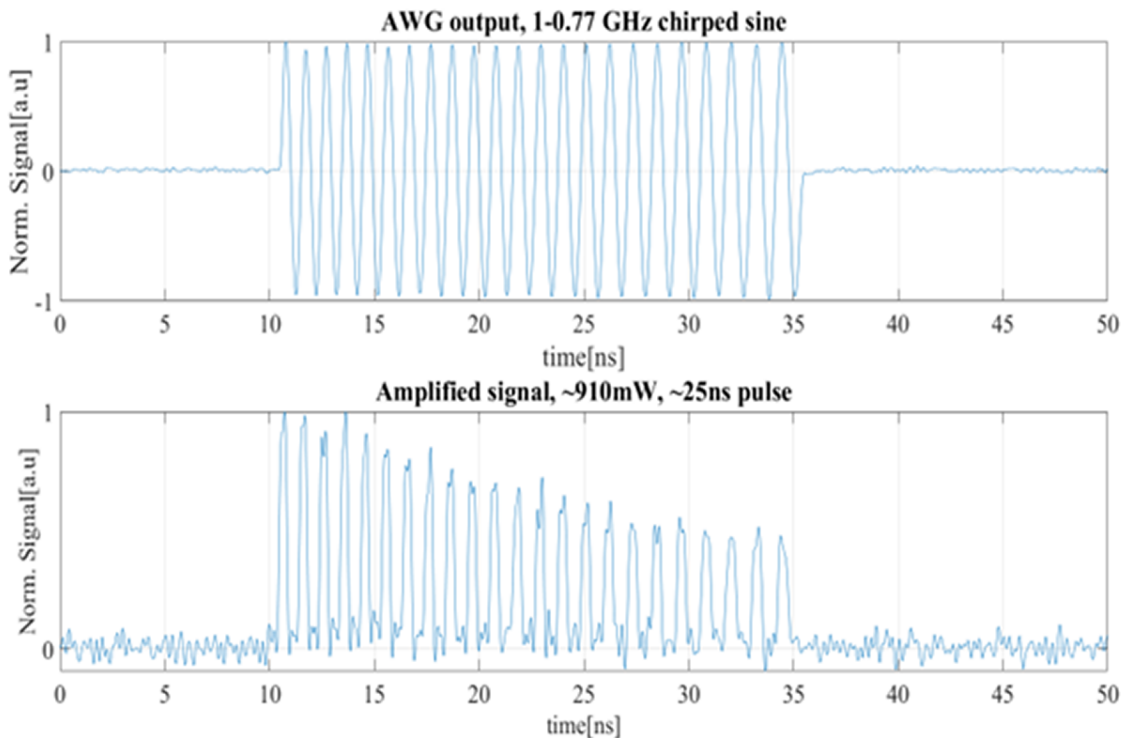


Figure 4. Electronic signal from the AWG (top) chirped from 1 to 0.77 GHz, and amplified optical pulse at 400 Hz repetition rate and averaged power of 910 mW.

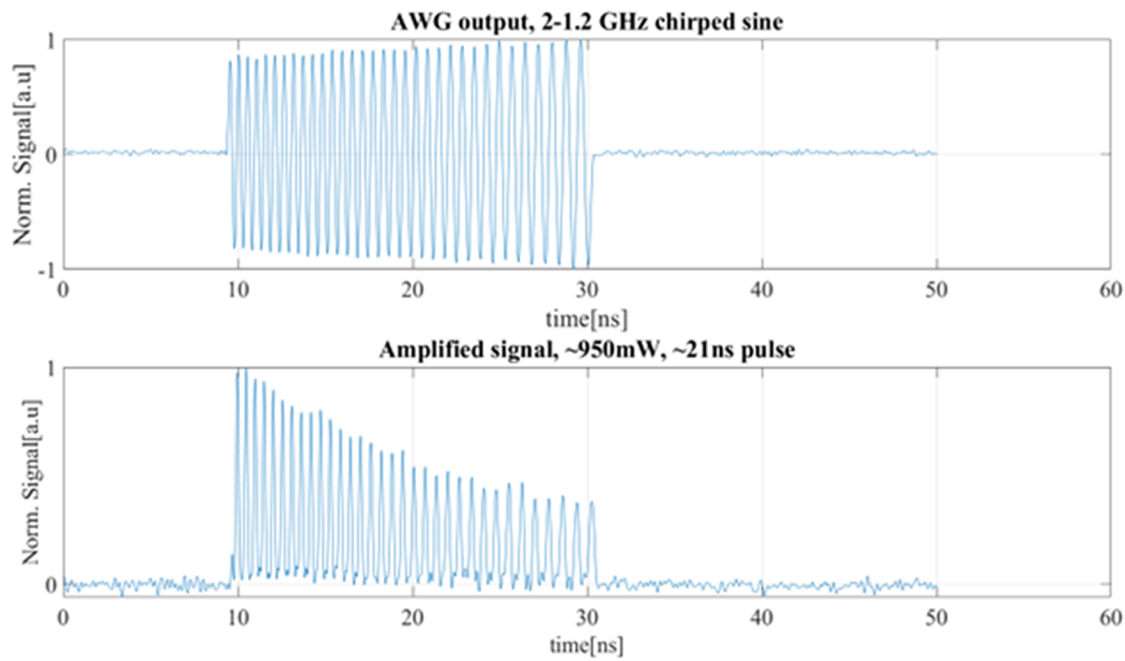


Figure 5. The same as Figure 4, but for frequencies spanning from 2 to 1.2 GHz.

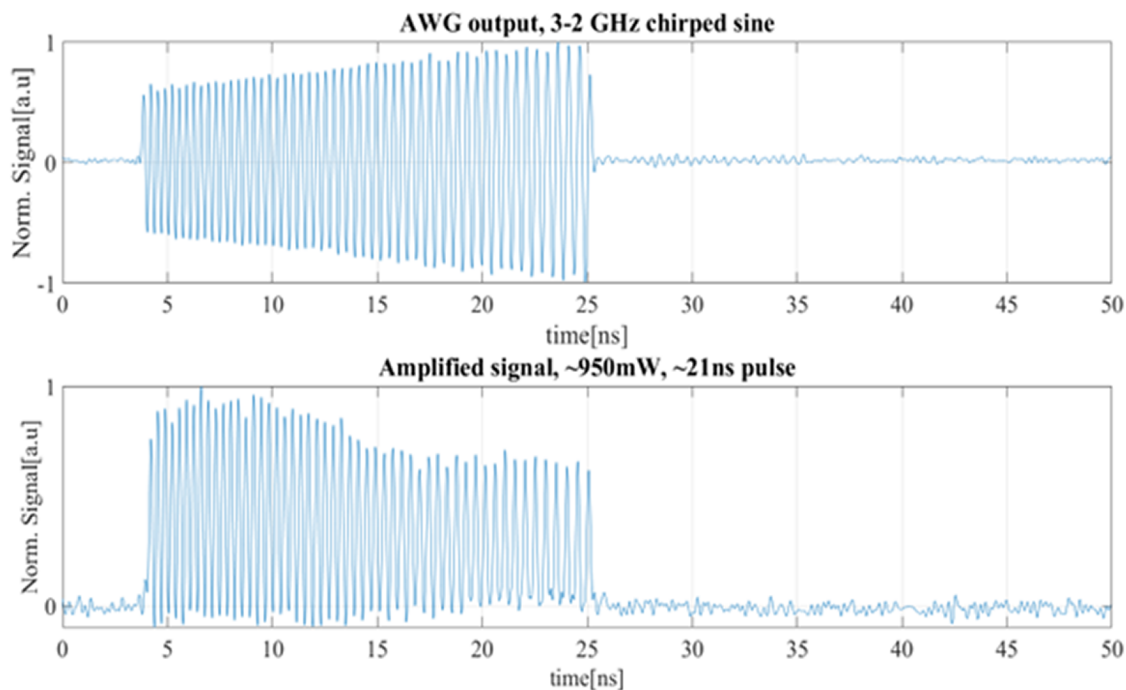


Figure 6. The same as Figures 4 and 5, but for frequencies spanning from 3 to 2 GHz.

If we look at the AR threshold conditions that are given in Figure 1 we see that 2.5 mJ per pulse would be enough if we focus the beam into a spot size of 30–35 μm . At such a spot size, the plane wave approximation in our previous work^[12] is questionable and we have to revisit our analysis while taking into account the finite width of the beam. Detailed analysis is given in the Appendix, and here we present the main results only. The charge distribution

inside the plasma yields potential ϕ . To account for the finite width of the laser and the plasma wave we assume $\phi = \phi(x)(1 - \frac{q^2 r^2}{4})$ for any $r < r_{\text{max}} = \frac{2}{q}$. This q parameter measures the tightness of the laser and plasma waves. Our goal in the appendix is to calculate the AR threshold as a function of this q parameter and compare it with the case of the plane wave approximation ($q \rightarrow 0$). Figure 7 shows the ratio $\varepsilon_{\text{th}}(q)/\varepsilon_{\text{th}}(q=0)$. It illustrates that only at tight

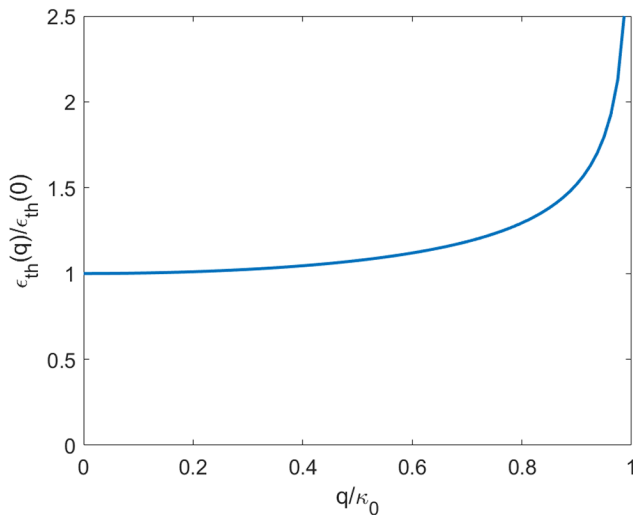


Figure 7. The ratio between the AR threshold for the finite beam width to the AR threshold for the case of a plane wave. Here, $q = 2/r_{\max}$ and κ_0 is the absolute value of the plane-wave wave-vector. It shows that only at tight focusing ($q/\kappa_0 > 0.7$) does the finite beam width start to play a significant role.

focusing ($q/\kappa_0 > 0.7$) does the finite width of the beam start to play a significant role and raise the AR threshold. In the parameter space calculated above (i.e., $r_{\max} \cong 30\text{--}35 \mu\text{m}$) we can safely use the AR threshold given in our previous work^[12].

To conclude, we have analyzed the available parameter space for the AR excitation of nonlinear ion acoustic waves and built the required chirped amplitude-modulated laser that could drive the ion acoustic waves. The shape of the laser pulses is determined by an AWG with pulse duration spanning from a few ns to approximately 30–35 ns. We showed amplitude modulation spanning from a few hundred MHz and up to 3 GHz. The energy per pulse is up to 3 mJ, enough to be above the AR threshold.

Appendix. Autoresonance excitation of SIAWs by a finite-width laser

Following a similar path as in Ref. [12], we start with the fluid model plasma equations and assume cold ions and hot electrons. We also assume a Boltzmann distribution for the electrons, thus $n_e = n_0 e^{\phi + \phi_d}$ where ϕ is the total potential due to charge distribution and ϕ_d is the driving potential. We write the ion fluid equations and Poisson’s equation within the cold ion limit:

$$n_{it} + (n_i v)_x = 0, \tag{2}$$

$$v_t + v v_x = -\frac{e}{m_i} \phi_x, \tag{3}$$

$$\nabla^2 \phi = 4\pi (n_e - n_i), \tag{4}$$

where the x and t subscripts represent a partial derivative in space and time, respectively, and n_e and n_i are the electron and ion densities, respectively. Now, to account for the finite wave width, we are looking for a solution for ϕ of the following form:

$$\phi = \phi(x) \left(1 - \frac{q^2 r^2}{4}\right) \quad \text{for } r < r_{\max} = \frac{2}{q}, \tag{5}$$

where $\phi(x)$ is the value of ϕ on axis ($r = 0$). With this assumption, Equation (4) becomes the following:

$$\phi_{xx} = q^2 \phi + 4\pi e [n_0 e^{e(\phi + \phi_d)/k_B T_e} - n_i]. \tag{6}$$

We convert all variables and parameters in Equations (2), (3) and (6) and hereafter into a dimensionless form, such that the time, the position and the velocities are normalized with respect to the inverse ion plasma frequency $\omega_i = \left(\frac{4\pi n_0 e^2}{m_i}\right)^{1/2}$, $\omega_i^{-1} = \sqrt{\frac{m_i}{4\pi n_0 e^2}}$, the Debye length $\lambda_D = \left(\frac{k_B T_e}{4\pi n_0 e^2}\right)^{1/2}$ and the modified ion thermal velocity $v_{T_i} = \left(\frac{k_B T_e}{m_i}\right)^{1/2}$. The plasma density and the electric potential are normalized with respect to the unperturbed plasma density and $\frac{k_B T_e}{e}$, respectively.

This yields the dimensionless set of ion equations:

$$n_t + (nu)_x = 0, \tag{7}$$

$$u_t + uu_x = -\phi_x, \tag{8}$$

$$\phi_{xx} = q^2 \phi + e^{\phi + \phi_d} - n. \tag{9}$$

Our goal is to find the AR threshold under finite wave width conditions. Next, we introduce two additional auxiliary potentials that are defined as follows:

$$u = \psi_x, \tag{10}$$

$$n = 1 + \sigma_x. \tag{11}$$

Then Equations (7)–(9) become the following:

$$\sigma_{xt} + \psi_{xx} (1 + \sigma_x) + \psi_x \sigma_{xx} = 0, \tag{12}$$

$$\psi_{xt} + \psi_x \psi_{xx} = -\phi_x, \tag{13}$$

$$\phi_{xx} = q^2 \phi + e^{\phi + \phi_d} - 1 - \sigma_x. \tag{14}$$

This system satisfies a variational principle $\delta \left(\int \mathcal{L} dx dt\right) = 0$, where the Lagrangian density for the three potentials σ, ψ, ϕ is as follows:

$$\mathcal{L} = \frac{1}{2}\phi_x^2 + \frac{1}{2}q^2\phi^2 + e^{\phi+\phi_d} - \frac{1}{2}(\psi_t\sigma_x + \psi_x\sigma_t) - \left(\frac{1}{2}\psi_x^2 + \phi\right)(1 + \sigma_x). \quad (15)$$

Here, we expand the exponential term in a Taylor series up to the fourth order in ϕ and to linear order in ϕ_d (assuming ϕ_d is small):

$$e^{\phi+\phi_d} \approx 1 + \phi_d + \phi\phi_d + V(\phi), \\ V = \phi + \frac{1}{2}\phi^2 + \frac{1}{6}\phi^3 + \frac{1}{24}\phi^4 + O(\phi^5). \quad (16)$$

The reason for expanding up to the fourth order in ϕ is that the third- and fourth-order terms contribute equally to the nonlinear self-frequency of an anharmonic oscillator^[25].

After neglecting the $1 + \phi_d$ (as it is not contributing to the dynamics), the Lagrangian density is as follows:

$$\mathcal{L} \approx \frac{1}{2}\phi_x^2 + \frac{1}{2}q^2\phi^2 + \phi\phi_d + V(\phi) - \frac{1}{2}(\psi_t\sigma_x + \psi_x\sigma_t) - \left(\frac{1}{2}\psi_x^2 + \phi\right)(1 + \sigma_x). \quad (17)$$

To proceed with our analysis, we make the following ansatz:

$$\sigma = A_1(t) \sin kx + A_2(t) \sin 2kx, \quad (18)$$

$$\psi = B_1(t) \cos kx + B_2(t) \cos 2kx, \quad (19)$$

$$\phi = C_0(t) + C_1(t) \cos kx + C_2(t) \cos 2kx, \quad (20)$$

where A_1, B_1 and C_1 are first-order perturbation terms, and all other terms are second-order perturbation. As for the time dependence of the first-order terms, we assume the following:

$$A_1 = \frac{a}{k} \cos \omega t, \quad B_1 = -\frac{b}{k} \sin \omega t, \quad C_1 = c \cos \omega t, \quad (21)$$

where a, b and c are constants.

To find the time dependence of the second-order terms, we substitute Equations (18)–(20) into Equation (17), ignore the driving term, and spatially average. This yields the averaged Lagrangian density $\Lambda = \Lambda_2 + \Lambda_4$:

$$\Lambda_2 = \frac{1}{4}(1 + q^2 + k^2)C_1^2 - \frac{k}{4}(A_1B_{1t} - B_1A_{1t}) - \frac{k^2}{4}B_1^2 - \frac{1}{2}kA_1C_1, \quad (22)$$

$$\Lambda_4 = \left(\frac{1}{4} + \frac{q^2}{4} + k^2\right)C_2^2 + \left(\frac{1}{2} + \frac{q^2}{2}\right)C_0^2 + C_1^2\left(\frac{1}{8} + \frac{1}{4}C_0 + \frac{1}{64}C_1^2\right) + \frac{k}{2}(A_{2t}B_2 - A_2B_{2t} - A_2C_2) - B_2^2k^2 + \frac{k^3}{2}\left(\frac{1}{2}A_2B_1^2 - A_1B_1B_2\right). \quad (23)$$

Using this averaged Lagrangian density, we get the following Euler–Lagrange equations for C_0, A_2, B_2 and C_2 :

$$B_{2t} = \frac{k^2}{4}B_1^2 - C_2, \quad (24)$$

$$A_{2t} = \frac{k^2}{2}A_1B_1 + 2kB_2, \quad (25)$$

$$C_0 = -\frac{C_1^2}{4(1 + q^2)}, \quad (26)$$

$$C_2 = \frac{kA_2 - C_1^2/8}{1/2 + 2k^2 + q^2/2}. \quad (27)$$

To further simplify this set of equations, we define two additional constants:

$$r = \frac{c^2}{8(1 + 4k^2 + q^2)} + \frac{b^2}{8}, \quad p = \frac{c^2}{8(1 + 4k^2 + q^2)} - \frac{b^2}{8}, \quad (28)$$

so that Equation (24) becomes the following:

$$B_{2t} = r + p \cos 2\omega t - \frac{2k}{1 + 4k^2 + q^2}A_2. \quad (29)$$

We can now try the following ansatz:

$$A_2 = A + a_2 \cos 2\omega t, \quad B_2 = b_2 \sin 2\omega t, \quad (30)$$

yielding the following:

$$-2\omega a_2 = -\frac{ab}{4} + kb_2, \quad (31)$$

$$r = \frac{2kA}{1 + 4k^2 + q^2}, \quad (32)$$

$$p = 2\omega b^2 + \frac{2ka_2}{1 + 4k^2 + q^2}, \quad (33)$$

$$C_2 = C + c_2 \cos 2\omega t. \quad (34)$$

This solution completes the weakly nonlinear ansatz (Equations (18)–(20)) for the finite-width SIAW. To account for the slowly varying frequency, we introduce phase $\theta = \int \omega dt$ instead of ωt :

$$\sigma = a_1 \cos \theta \sin kx + (A + a_2 \cos 2\theta) \sin 2kx, \quad (35)$$

$$\psi = b_1 \sin \theta \cos kx + b_2 \sin 2\theta \cos 2kx, \quad (36)$$

$$\phi = c_0 \cos^2 \theta + c_1 \cos \theta \cos kx + (C + c_2 \cos 2\theta) \cos 2kx. \quad (37)$$

At this stage, we apply Whitham's averaged variational approach. To this end, we assume that all amplitudes are slow functions of time, substitute Equations (35)–(37) back

into the approximated Lagrangian equation (Equation (17)), average it over one temporal and one spatial period and get the averaged second- and fourth-order Lagrangian densities:

$$\Lambda_2 = \frac{1}{8} [c_1^2 (1 + q^2) - 2ka_1c_1 - k^2 (b_1^2 - c_1^2) - 2k\omega a_1 b_1], \tag{38}$$

$$\begin{aligned} \Lambda_4 = & (1 + q^2) \left(\frac{1}{4} C^2 + \frac{3}{16} c_0^2 + \frac{1}{8} c_2^2 \right) + \frac{1}{32} c_1^2 (3c_0 + c_2 + 2C) \\ & + \frac{3}{512} c_1^4 - \frac{k^2}{2} (b_2^2 - c_2^2 - 2C^2) \\ & - \frac{k^3}{8} b_1 \left(\frac{1}{2} a_2 b_1 - A b_1 + a_1 b_2 \right) - k \left(\omega a_2 b_2 + AC + \frac{1}{2} a_2 c_2 \right). \end{aligned} \tag{39}$$

We also reintroduce the driving potential:

$$\phi_d = 2\epsilon \cos(\theta_d) \cos(kx) = 2\epsilon \cos(\theta + \Phi) \cos(kx). \tag{40}$$

At this stage, we assume that the system and driving force are phase-locked in the weakly nonlinear regime; thus, the AR can take place if $\Phi(t)$ is a slow phase mismatch. When multiplied by ϕ and averaged (over one spatial and one temporal period) we are left with the driving Lagrangian density:

$$\Lambda_d = \frac{1}{2} \epsilon c_1 \cos \Phi, \tag{41}$$

and the dynamics of the system is governed by the total averaged Lagrangian density:

$$\Lambda = \Lambda_2 + \Lambda_4 + \Lambda_d, \tag{42}$$

where Λ is a function of all slow amplitudes and θ entering the Lagrangian density via the time-dependent frequency $\omega = \theta_t$ and the slow phase mismatch $\Phi = \theta_d - \theta$. By taking variations via Λ in Equation (42) with respect to $\{c_0, a_2, b_2, c_2, A, C\}$ we find all the second-order coefficients as functions of the first-order terms. These coefficients can be substituted back into Λ , which can then be used to take variations with respect to the first-order terms $\{a_1, b_1, c_1, \Phi\}$. This yields the following solutions:

$$b_1 = -\frac{2c_1 + k^2 b_1 b_2}{2\omega} = -\frac{2c_1 + Q}{2\omega}, \tag{43}$$

$$\begin{aligned} a_1 = & \frac{2kc_1 + kk^2 b_1 b_2 - \omega k^2 [b_1 (a_2 - 2A) + a_1 b_2]}{2\omega^2} \\ = & \frac{2kc_1 + kQ - \omega R}{2\omega^2}, \end{aligned} \tag{44}$$

where

$$Q = k^2 b_1 b_2, \quad R = k^2 [b_1 (a_2 - 2A) + a_1 b_2]. \tag{45}$$

Next, the variations with respect to c_1 and Φ yield the following:

$$\begin{aligned} & [c_1 (1 + q^2) - ka_1 + c_1 k^2] + \frac{1}{4} c_1 (3c_0 + c_2 + 2C) \\ & = -\frac{3}{32} c_1^3 + 2\epsilon \cos \Phi, \end{aligned} \tag{46}$$

$$\frac{d}{dt} \left(-\frac{1}{4} ka_1 b_1 - ka_2 b_2 \right) = \frac{1}{2} \epsilon c_1 \sin \Phi. \tag{47}$$

To the lowest significant order, Equation (47) becomes the following:

$$k[a_1 b_1]_t = -2\epsilon c_1 \sin \Phi. \tag{48}$$

Furthermore, Q and R are of the third order, and the linear approximations for a_1 and b_1 are as follows:

$$a_1 \approx \frac{k}{\omega^2} c_1, \quad b_1 \approx -\frac{c_1}{\omega}. \tag{49}$$

By substituting this into Q and R we get the following:

$$Q \approx c_1^3 \frac{\frac{k^6}{\omega^4} + \frac{k^4}{\omega^2} (1 + q^2 + 4k^2) - k^2}{16[-k^2 + \omega^2 (1 + q^2 + 4k^2)]}, \tag{50}$$

$$\begin{aligned} R \approx & \frac{c_1^3 \{-2k^7/\omega^2 (2 + q^2 + 4k^2) + k^5 [3/\omega^2 - 1 - 2(1 + q^2 + 4k^2)] (1 + q^2 + 4k^2)\}}{16\omega[-k^2 + \omega^2 (1 + q^2 + 4k^2)]} \\ & + \frac{c_1^3 [-k^3 + 2k\omega^2 (1 + q^2 + 4k^2)]}{16\omega[-k^2 + \omega^2 (1 + q^2 + 4k^2)]}. \end{aligned} \tag{51}$$

Thus, after the substitution of Equations (49)–(51) into Equations (48) and (46), we have the following:

$$c_{1t} \approx -\frac{\epsilon \omega^3}{k^2} \sin \Phi, \tag{52}$$

$$\left[\frac{k^2}{\omega^2} - (1 + q^2 + k^2) \right] c_1 = -Nc_1^3 + 2\epsilon \cos \Phi, \tag{53}$$

where we use the following new parameters:

$$h = 32 (1 + q^2) \omega^6 [-k^2 + (1 + 4k^2 + q^2) \omega^2], \tag{54}$$

$$\begin{aligned} J = & 4k^8 (1 + q^2) - [-12k^2 - 4 + (-1 + 3q^2 + 12k^2) q^2] \omega^8 \\ & - k^2 [16k^2 (1 + q^2) + (7 + 5q^2 + 4q^4)] \omega^6 \\ & + 7 (1 + q^2) k^6 (1 + q^2 + 4k^2) \omega^2 \\ & - 2k^4 (1 + q^2) [(2 + 2q^2 + q^4) + 8k^2 (1 + q^2) + 16k^4] \omega^4, \end{aligned} \tag{55}$$

$$N = \frac{J}{h}. \tag{56}$$

Notice that the term in the square brackets in Equation (53) yields the ion acoustic wave dispersion relation for the case of a finite-width wave:

$$\omega_a = \frac{k}{(1+q^2+k^2)^{1/2}}. \quad (57)$$

The capture into AR occurs during the weakly nonlinear regime, meaning that the driving frequency is close to the linear frequency:

$$\omega = \omega_a + \Delta\omega, \quad \Delta\omega \ll \omega_a. \quad (58)$$

Then Equation (53) becomes the following:

$$\left[\frac{k^2}{(\omega_a + \Delta\omega)^2} - (1+q^2+k^2) \right] c_1 = -Nc_1^3 + 2\epsilon \cos \Phi, \quad (59)$$

which by expanding around ω_a yields the following:

$$\Delta\omega \approx -\frac{\omega^3}{2k^2} \left(-Nc_1^2 + \frac{2\epsilon}{c_1} \cos \Phi \right). \quad (60)$$

Since

$$\omega_d = \omega + \Phi_d, \quad \omega_d = \omega_a - \alpha t \rightarrow \Phi_t = \Delta\omega + \alpha t, \quad (61)$$

by writing $\beta = \frac{\omega^3}{2k^2} N$ we get the following:

$$\Phi_t \approx \beta c_1^2 + \alpha t - \frac{\epsilon}{c_1} \frac{\omega^3}{k^2} \cos \Phi. \quad (62)$$

Then, as shown in Ref. [2], the critical amplitude for transition to AR is as follows:

$$\begin{aligned} \epsilon_{\text{th}} &= 0.41 \frac{k^2 \alpha^{3/4}}{\omega_a^3 \beta^{1/2}} \\ &= 5.86 \alpha^{3/4} (1+k^2+q^2)^{9/4} (1+q^2)^{1/2} \\ &\quad \cdot \left\{ k^{1/2} \left[27k^6(q^2+1)^2 + 9k^4(q^2+1)(7q^4+14q^2+5) \right. \right. \\ &\quad \left. \left. + 3k^2(15q^8+60q^6+82q^4+41q^2+10) \right. \right. \\ &\quad \left. \left. + 9q^{10} + 45q^8 + 84q^6 + 72q^4 + 28q^2 + 4 \right]^{1/2} \right\}^{-1}. \end{aligned} \quad (63)$$

In the case of $q = 0$, that is, for the plane wave assumption, this critical amplitude agrees with the previous result^[12]:

$$\epsilon_{\text{th}}(q=0) = \frac{5.68 \alpha^{3/4} (1+k^2)^{9/4}}{k^{1/2} (27k^6 + 45k^4 + 30k^2 + 4)^{1/2}}. \quad (64)$$

The plot of Equation (63) in Figure 7 shows that the radial effect starts to play a significant role only in the tight focusing limit and we can safely obtain AR in our system within moderate focusing conditions.

Acknowledgements

This work was supported by NSF-BSF (Grant No. 1803874/2017635) and US-Israel Binational Science Foundation (Grant No.2020233).

References

1. V. M. Malkin, G. Shvets, and N. J. Fisch, *Phys. Rev. Lett.* **82**, 4448 (1999).
2. A. A. Andreev, C. Riconda, V. T. Tikhonchuk, and S. Weber, *Phys. Plasmas* **13**, 053110 (2006).
3. G. Lehmann and K. H. Spatschek, *Phys. Rev. Lett.* **116**, 225002 (2016).
4. Y. Katzir, Y. Ferber, J. R. Penano, R. F. Hubbard, P. Sprangle, and A. Zigler, *Opt. Express* **21**, 5077 (2013).
5. I. Y. Dodin and N. J. Fisch, *Phys. Rev. Lett.* **88**, 165001 (2002).
6. M. R. Edwards, V. R. Munirov, A. Singh, N. M. Fasano, E. Kur, N. Lemos, J. M. Mikhailova, J. S. Wurtele, and P. Michel, *Phys. Rev. Lett.* **128**, 065003 (2022).
7. P. Michel, L. Divol, D. Turnbull, and J. D. Moody, *Phys. Rev. Lett.* **113**, 205001 (2014).
8. D. Turnbull, P. Michel, T. Chapman, E. Tubman, B. B. Pollock, C. Y. Chen, C. Goyon, J. S. Ross, L. Divol, N. Woolsey, and J. D. Moody, *Phys. Rev. Lett.* **116**, 205001 (2016).
9. G. Lehmann and K. H. Spatschek, *Phys. Rev. E* **97**, 063201 (2018).
10. P. Michel, L. Divol, E. A. Williams, S. Weber, C. A. Thomas, D. A. Callahan, S. W. Haan, J. D. Salmonson, S. Dixit, D. E. Hinkel, M. J. Edwards, B. J. MacGowan, J. D. Lindl, S. H. Glenzer, and L. J. Suter, *Phys. Rev. Lett.* **102**, 025004 (2009).
11. Y. X. Wang, S. M. Weng, P. Li, Z. C. Shen, X. Y. Jiang, J. Huang, X. L. Zhu, H. H. Ma, X. B. Zhang, X. F. Li, Z. M. Sheng, and J. Zhang, *High Power Laser Sci. Eng.* **11**, e37 (2023).
12. L. Friedland, G. Marcus, J. S. Wurtele, and P. Michel, *Phys. Plasmas* **26**, 092109 (2019).
13. J. Fajans and L. Friedland, *Amer. J. Phys.* **69**, 1096 (2001).
14. G. Marcus, L. Friedland, and A. Zigler, *Phys. Rev. A* **69**, 013407 (2004).
15. G. Marcus, L. Friedland, and A. Zigler, *Phys. Rev. A* **72**, 033404 (2005).
16. G. Marcus, A. Zigler, D. Eger, A. Bruner, and A. Englander, *J. Opt. Soc. Am. B* **22**, 620 (2005).
17. G. Marcus, A. Zigler, and L. Friedland, *Europhys. Lett.* **74**, 43 (2006).
18. L. Friedland, *Phys. Rev. E* **59**, 4106 (1999).
19. J. Fajans, E. Gilson, and L. Friedland, *Phys. Rev. Lett.* **82**, 4444 (1999).
20. L. Friedland and A. G. Shagalov, *Phys. Rev. Lett.* **81**, 4357 (1998).
21. L. Friedland, *Astrophys. J.* **547**, L75 (2001).
22. B. Stann, B. C. Redman, W. Lawler, M. Giza, J. Dammann, and K. Krapels, *Proc. SPIE* **6550**, 655005 (2007).
23. W. Kochner, *Solid State Laser Engineering*, 6th ed. (Springer, New York, 2006).
24. <http://www.rezonator.orion-project.org/>.
25. L. D. Landau and E. M. Lifshitz, *Mechanics*, 3rd ed. (Elsevier, Butterworth-Heinemann, 2011).